JOURNAL OF COMPUTATIONAL PHYSICS 44, 359–376 (1981)

Calculation of the Rotational Normal Modes of Oceans and Lakes with General Orthogonal Coordinates*

JOHN R. BENNETT AND DAVID J. SCHWAB

Great Lakes Environmental Research Laboratory, NOAA, Ann Arbor, Michigan 48104

Received August 14, 1980; revised October 12, 1981

A finite-difference method for computing the frequency and structure of the rotational modes of oscillation of enclosed seas is tested against known solutions for: (1) a circular basin with a parabolic depth law, (2) a circular, flat basin with a linear variation of the Coriolis parameter, and (3) an elliptic paraboloid. Several higher modes of the elliptic paraboloid are also calculated. The method uses the non-divergent assumption and solves the barotropic vorticity equation in general orthogonal coordinates generated by a conformal map of the shoreline onto the unit circle. The numerical procedure for calculating the conformal map of an arbitrarily shaped basin is presented.

1. INTRODUCTION

For computation of the currents of oceans and lakes, it is essential to take into account the shape of the shoreline and the variations in depth. The simplest numerical method for this is to lay a rectangular finite-difference grid over the lake and mask out the land grid points. Much is known about the accuracy of these schemes, and it is straightforward to formulate computationally stable, explicit finite-difference schemes, that conserve mass, momentum, and energy.

For the simplest flow problem, the prediction of storm surges in a shallow lake, this method seems satisfactory. Schwab [1, 2] showed that for Lake Erie the finite-difference method using a 10-km grid worked as well as a finite element model, a 5-km grid finite-difference model, or an empirical transfer function technique. For a related problem, the calculation of the gravitational oscillations of small closed basins, this type of grid is also adequate [3, 4]. Undoubtedly, a major reason for the success of these methods is that water level has a much simpler spatial distribution than current does. Even for an irregular lake the water level displacement due to the wind is similar to the classical setup solution for a constant depth lake, and the seiches have large spatial scales and are not influenced by the details of the shoreline shape or the topography.

In contrast, current patterns are strongly influenced by the details of the lake's shape. This is particularly true for deep lakes, where Coriolis, inertial, buoyancy, and

* GLERL Contribution No. 230.

0021-9991/81/120359-18$02.00/0

frictional forces can combine to produce complex coastal boundary layers. The influence of grid resolution on computed currents is most clearly illustrated by the solutions of Bennett [5]. Even though these calculations were done for a circular lake and used cylindrical coordinates, thus eliminating the problem of resolving the shape of the lake, the currents were shown to be strongly dependent on the resolution of the offshore coordinate.

For rotational oscillations, it is possible to have nearly the same frequency for modes of very different scales. An ocean may have a large-scale Rossby mode and a small-scale topographic mode trapped near a seamount, but the periods of the two may be equal. In fact, many oceans and lakes have such complex shapes that it may not be useful to look for rotational modes in data or to try to compute them. In this respect, these modes are fundamentally different from the gravitational modes, for which the period increases as the wavelength increases. However, for basins of fairly simple shape, it is reasonable to expect to see wind-driven current patterns that look like the large-scale normal modes. These modes are interesting in their own right and we feel that the accuracy of computing them will give a good indication of how well the finite-difference schemes will compute wind-driven currents. We tried to compute them explicitly for a rectangular grid but failed; we were only able to reproduce the simplest mode of a circular paraboloid. We concluded that it is necessary to use general orthogonal coordinates. The "offshore" and the "longshore" coordinates are generated by a conformal map of the lake onto the unit circle. We will test the accuracy of the method by computing the rotational normal modes of some simple shapes and comparing the computed frequencies and structures to exact solutions.

2. Basic Equations

If friction and density variations are neglected, small amplitude displacements of a shallow lake from a motionless state can be described in terms of the vertically averaged horizontal velocity and the displacement of the free surface, η. Furthermore, for oscillations with frequencies less than the Coriolis parameter, f, it is permissible to neglect the variation of the free surface in the continuity equation as long as the basin is not as wide as c/f, where c is the velocity of long gravity waves in a non-rotating system. The effect of the free surface variation is then felt only through the variation of the hydrostatic pressure, $g\eta$. With these simplifications, the normal modes depend only on the Coriolis parameter and the shape of the basin, and not on gravity, density, or the maximum depth; thus, these parameters will all be assumed equal to unity. As spatial coordinates we will use the orthogonal curvilinear coordinates ρ and ϕ. The equations of motion can then be written

$$\frac{\partial u}{\partial t} - fv = -\frac{1}{M_\rho}\frac{\partial \eta}{\partial \rho}, \tag{2.1}$$

$$\frac{\partial v}{\partial t} + fu = -\frac{1}{M_\phi}\frac{\partial \eta}{\partial \phi}. \tag{2.2}$$

Here u and v are the components of horizontal velocity in the two locally perpendicular directions ρ and ϕ, M_ρ and M_ϕ are metric functions giving physical distance per unit of ρ and ϕ, and t is time. The continuity equation is

$$\frac{\partial(uM_\phi H)}{\partial\rho}+\frac{\partial(vM_\rho H)}{\partial\phi}=0, \tag{2.3}$$

where H is the depth. Because of this constraint, the velocity components can be described by a single scalar variable, ψ, the stream function.

$$u=\frac{-1}{HM_\phi}\frac{\partial\psi}{\partial\phi}, \qquad v=\frac{1}{HM_\rho}\frac{\partial\psi}{\partial\rho}. \tag{2.4}$$

At this point the formulation is very general; ρ and ϕ are any orthogonal coordinates. They could be the Cartesian coordinates of a local plane approximation to the earth's surface or they could be longitude and latitude. For Cartesian coordinates the metric functions M_ρ and M_ϕ can be constants. For longitude and latitude, M_ρ is the distance between the meridians (a function of latitude) and M_ϕ is simply the radius of the earth. The appropriate boundary condition for any closed basis is that there be no flow through the coast; i.e., that ψ is a constant on any boundary. If this boundary is mapped onto the unit circle and ρ and ϕ are radial and azimuthal polar coordinates then this condition is $\psi=0$ on $\rho=1$. From these and the definition of potential vorticity,

$$P=\frac{f}{H}, \tag{2.5}$$

Eqs. (2.1) and (2.2) can be written

$$\frac{\partial}{\partial t}\left(\frac{-M_\rho}{HM_\phi}\frac{\partial\psi}{\partial\phi}\right)-P\frac{\partial\psi}{\partial\rho}=-\frac{\partial\eta}{\partial\rho}, \tag{2.6}$$

$$\frac{\partial}{\partial t}\left(\frac{M_\phi}{HM_\rho}\frac{\partial\psi}{\partial\rho}\right)-P\frac{\partial\psi}{\partial\phi}=-\frac{\partial\eta}{\partial\phi}. \tag{2.7}$$

An alternative form can be obtained by eliminating η,

$$\frac{\partial}{\partial t}\left[\frac{\partial}{\partial\rho}\left(\frac{M_\phi}{HM_\rho}\frac{\partial\psi}{\partial\rho}\right)+\frac{\partial}{\partial\phi}\left(\frac{M_\rho}{HM_\phi}\frac{\partial\psi}{\partial\phi}\right)\right]=\frac{\partial\psi}{\partial\phi}\frac{\partial P}{\partial\rho}-\frac{\partial\psi}{\partial\rho}\frac{\partial P}{\partial\phi}. \tag{2.8}$$

This equation, the barotropic vorticity equation, relates the time rate of change of vorticity to the rate at which the flow crosses contours of potential vorticity. If the potential vorticity is uniform, the flow is steady. Equation (2.8) has normal mode solutions of the form

$$\psi(\rho,\phi,t)=\mathrm{Re}[\hat{\psi}(\rho,\phi)e^{i\sigma t}], \tag{2.9}$$

where the frequency, σ, is real. If Eq. (2.9) is used in Eq. (2.8) the result is

$$i\sigma\left[\frac{\partial}{\partial\rho}\left(\frac{M_\phi}{HM_\rho}\frac{\partial\hat{\psi}}{\partial\rho}\right)+\frac{\partial}{\partial\phi}\left(\frac{M_\rho}{HM_\phi}\frac{\partial\hat{\psi}}{\partial\phi}\right)\right]=\frac{\partial\hat{\psi}}{\partial\phi}\frac{\partial P}{\partial\rho}-\frac{\partial\hat{\psi}}{\partial\rho}\frac{\partial P}{\partial\phi} \tag{2.10}$$

which has the form of a generalized eigenvalue problem for the eigenvalue, $i\sigma$, and the eigenvector, $\hat{\psi}$.

The rotational oscillations computed here can be considered to be of two types, those due to variation in the earth's vorticity, f, and those due to variations in depth. Since f varies as the sine of the latitude, its variation is only significant for an ocean basin. For small lakes and seas, the depth variation is more important. The numerical technique developed in the following sections will be tested against exact solutions of this equation for both types of oscillations.

3. Generation of Orthogonal Coordinates by Conformal Mapping

This section describes a practical method for conformally mapping a closed domain onto the interior of the unit circle. The purpose of the conformal map is to generate a coordinate system in physical space that has the following two properties. First, the system is locally orthogonal. This allows us to use Eqs. (2.6) and (2.7) without the addition of the terms arising from differentiating the coordinate system. Second, the shoreline of the basin is an isoline of the coordinate system. Because of this property, the boundary condition that the flow is parallel to the shoreline can be incorporated very naturally into finite-difference approximations to (2.6) and (2.7).

Let the radial and azimuthal coordinates in physical space be r and θ. The radial coordinate, r, has been nondimensionalized by the maximum radius for the basin, R. Let the transformed coordinates in the unit circle be ρ and ϕ. The transformation from the unit circle to physical space is expressed as a power series in terms of the transformed coordinates, i.e.,

$$z=\sum_{n=0}^{m}a_n w^n, \tag{3.1}$$

where $z=re^{i\theta}$ is a point in physical space and $w=\rho e^{i\phi}$ is a point in the unit circle. Equation (3.1) assigns a unique point in physical space to each point in the unit circle.

The coefficients a_n are determined numerically from a set of discrete points in physical space which are on the shoreline of the basin. The coordinates of the boundary points are $z_j=r_j e^{i\theta_j}$. These points are mapped onto the circumference of the unit circle ($\rho=1$) so that (3.1) becomes

$$z_j=\sum_{n=0}^{m}a_n e^{in\phi_j} \tag{3.2}$$

for boundary points. The transformed azimuthal coordinates of the boundary points, ϕ_j, can be calculated without knowledge of the expansion coefficients, a_n, with an iterative procedure described by Swinford [6]. The starting points for the procedure are the coordinates in physical space, $z_{j,i}$, normalized so that $|z_{j,i}| < 1$. The second subscript is used to indicate iteration number. These points are transformed by a recursion formula that produces points ever closer to the unit circle. The recursion for the iteration is

$$z_{j,k+1} = 1 - \frac{2 \log \alpha_k}{\log((z_{j,k} e^{-i\chi_k} - \alpha_k)/(z_{j,k} e^{-i\chi_k} - 1/\alpha_k))}, \tag{3.3}$$

where α_k and χ_k are the radial and azimuthal coordinates of the boundary point nearest the origin (farthest from the unit circle) at the kth iteration. Swinford [6] pointed out that (3.3) converges onto the unit circle such that $1 - \alpha_k = O(1/k)$. In practice, the iterations are carried out until $1 - \alpha_k < \delta$, where δ is a specified parameter. Because the conformal mapping of the domain onto the unit circle is unique, the convergence of (3.3) determines ϕ_j for each z_j.

If the ϕ_j were equally spaced on the unit circle, the functions would be numerically orthogonal and one could use a Fourier transform technique to calculate a_n. For unequally spaced ϕ_j, the a_n are determined by minimizing the error in (3.2) for successive values of m. If the series (3.2) is truncated at $m = 0$, we have

$$z_j = a_0. \tag{3.4}$$

The sum of the squared errors for l discrete points on the boundary weighted by arc length on the unit circle is

$$E^2 = \frac{1}{l} \sum_{j=1}^{l} (z_j - a_0)(z_j - a_0)^* \, |e^{i\phi_{j+1}} - e^{i\phi_{j-1}}|. \tag{3.5}$$

The condition for minimizing E^2 is

$$a_0 = \frac{1}{2\pi l} \sum_{j=1}^{l} z_j \, |e^{i\phi_{j+1}} - e^{i\phi_{j-1}}|. \tag{3.6}$$

Now let $m = 1$ and define

$$z_j' = z_j - a_0 = a_1 e^{i\phi_j}. \tag{3.7}$$

Then minimize

$$E^2 = \frac{1}{l} \sum_{j=1}^{l} (z_j' - a_1 e^{i\phi_j})(z_j' - a_1 e^{i\phi_j})^* \, |e^{i\phi_{j+1}} - e^{i\phi_{j-1}}| \tag{3.8}$$

to find

$$a_1 = \frac{1}{2\pi l} \sum_{j=1}^{l} z_j' e^{-i\phi_j} |e^{i\phi_{j+1}} - e^{i\phi_{j-1}}|. \tag{3.9}$$

This procedure works until the successive error terms continue to decrease only at the expense of the power series (3.2) diverging for some $z \neq z_j$ on the unit circle. A practical limit is $m \leqslant l/5$. This problem is equivalent to allowing a sufficient number of degrees of freedom for statistically reliable results in time series analysis.

An elliptic basin was chosen as a test case for the conformal mapping procedure described above. The analytic transformation of the interior of an ellipse to the interior of the unit circle is given in [7] as

$$z = \sin\left[\frac{\pi}{2D} sn^{-1}\left(\frac{w}{\sqrt{d}}, q\right)\right]. \tag{3.10}$$

Here sn^{-1} is the inverse of the Jacobi elliptic function with nome $q = ((\varepsilon - 1)/(\varepsilon + 1))^2$, where ε is the ratio of the major to the minor axis of the ellipse. The periods of the doubly periodic function sn are $4D$ and $2iD\sqrt{1-d^2}$. By using the power series expansions for sin and sn given in [8], we can find the first few coefficients of the expansion of z in terms of w. These are

$$\begin{aligned} a_0 &= a_2 = a_4 = 0, \\ a_1 &= \frac{\pi}{2D\sqrt{d}}, \\ a_3 &= \frac{a_1}{6d}\left[(1+d^2) - \left(\frac{\pi}{2D}\right)^2\right], \\ a_5 &= \frac{a_1}{4d^2}\left[\frac{(3+2d^2+3d^4)}{10} - \frac{(1+d^2)}{3}\left(\frac{\pi}{2D}\right)^2 + \frac{1}{30}\left(\frac{\pi}{2D}\right)^4\right]. \end{aligned} \tag{3.11}$$

To test the conformal mapping procedure, we calculated l discrete points on the boundary of an ellipse as

$$z_j = \sqrt{\frac{\varepsilon^2}{\varepsilon^2 - 1}} \cos\frac{2\pi j}{l} + i\sqrt{\frac{1}{\varepsilon^2 - 1}} \sin\frac{2\pi j}{l}. \tag{3.12}$$

The points were normalized so the $|z_j| < 1$, and (3.3) was applied iteratively until $1 - \alpha_k < 10^{-4}$. The a_n were then calculated with the original z_j up to $n = l/5$. The results for elliptical basins with $\varepsilon = 2$ and $\varepsilon = 3$ for various l are shown in Table I. Analytical coefficients were determined from (3.11) with the appropriate value of the

TABLE I

Computed and Analytic Expansion Coefficients for Elliptic Basins

$\varepsilon = 2$					
l	a_1	a_3	a_5	Iterations	Relative error
100	0.71194	0.17458	0.08223	309	0.026
200	0.70574	0.17590	0.08394	565	0.011
400	0.70275	0.17649	0.08482	999	0.006
Analytic	0.69970	0.17708	0.08571	—	—
$\varepsilon = 3$					
l	a_1	a_3	a_5	Iterations	Relative error
100	0.45770	0.13523	0.07475	284	0.140
200	0.44931	0.13399	0.07433	503	0.070
400	0.44524	0.13339	0.07421	857	0.045
800	0.44325	0.13309	0.07414	1513	0.019
Analytical	0.43823	0.13205	0.07376	—	—

nome q. The parameters d and D were calculated from the tables of elliptic functions in [8]. Relative error is computed as

$$E = \left[\frac{\sum_{j=1}^{l} (z_j - z_j')(z_j - z_j')^*}{\sum_{j=1}^{l} z_j z_j^*} \right]^{1/2}. \tag{3.13}$$

The number of iterations for convergence of (3.3) is also shown. The magnitudes of even-numbered coefficients and imaginary parts of all coefficients were at least three orders of magnitude smaller than a_1. For $\varepsilon = 3$ and $m = 800$, 5 minutes of CPU time was required on the CDC 6600 computer.

Since the mapping onto the unit circle is conformal, the contours of ρ in the physical plane are orthogonal to those of ϕ. For computational purposes, however, the grid points need not be equally spaced in ρ and ϕ. For the circular test cases, we chose to use $\rho' = \rho^2$ and $\phi' = \phi$, which, as Beardsley [9] pointed out, makes the number of grid points per unit area a constant. For the elliptical test case we chose $\rho' = \rho^2$. The values of ϕ were chosen so that at the shoreline the grid points were approximately equidistant in arc length. This seems to give a smooth distribution of grid points; but we can offer no general rules for choosing a grid.

4. Finite Differences

We constructed the finite-difference scheme with two criteria in mind. First, it should conserve energy so that there are no growing or decaying normal modes.

Second, it should be as accurate as possible. Energy conservation will be guaranteed by using one of the Arakawa [10, 11] methods. We will consider the two momentum equations, (2.6) and (2.7), to be the primary statement of the problem. The pressure, η, is a dummy variable to be eliminated by adding and subtracting finite-difference equations. For the central grid point in the conformal map, this will be done by summing the finite-difference equivalent of (2.7) around the center and requiring that η be single-valued. For all other points, it amounts to forming the equivalent of the vorticity equation, (2.8). One does not lose flexibility by introducing this dummy pressure since all the Arakawa's energy conserving schemes for the vorticity equation can be written in this manner.

Since this pressure is to be eliminated, there is no penalty for subtracting the quantity $\gamma\psi P$ from it, where γ is an arbitrary constant. Then Eqs. (2.6) and (2.7) can be rewritten as follows:

$$\frac{\partial}{\partial t}\left(\frac{-M_\rho}{HM_\phi}\frac{\partial\psi}{\partial\phi}\right) - (1-\gamma)P\frac{\partial\psi}{\partial\rho} + \gamma\psi\frac{\partial P}{\partial\rho} = -\frac{\partial\hat{\eta}}{\partial\rho}, \tag{4.1}$$

$$\frac{\partial}{\partial t}\left(\frac{+M_\phi}{HM_\rho}\frac{\partial\psi}{\partial\rho}\right) - (1-\gamma)P\frac{\partial\psi}{\partial\phi} + \gamma\psi\frac{\partial P}{\partial\phi} = -\frac{\partial\hat{\eta}}{\partial\phi}, \tag{4.2}$$

where $\hat{\eta} = \eta - \gamma\psi P$.

With appropriate finite-difference formulas for the terms on the left-hand side of these equations, all of Arakawa's energy conserving schemes correspond to a given

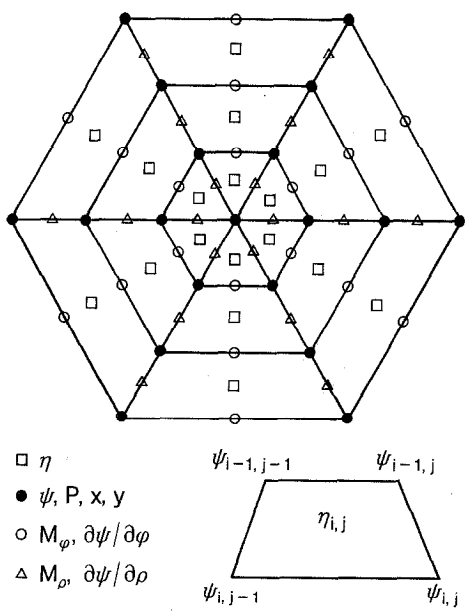

FIG. 1. Finite-difference grid in general orthogonal coordinates.

choice of γ. It is easiest to visualize the construction of these formulas with the aid of Fig. 1. This figure shows a simple finite-difference grid in which the radial coordinate is split into three equal segments and the azimuthal coordinate is split into six. We define the coordinates of the image point in the physical plane, x and y, at the solid circles. Although the metrics, M_ρ and M_ϕ, may be defined in a number of ways, we will use the simple definitions

$$\begin{aligned} M_\rho &= \sqrt{(x-x_{j-1})^2 + (y-y_{j-1})^2}, \\ M_\phi &= \sqrt{(x-x_{i-1})^2 + (y-y_{i-1})^2}, \end{aligned} \tag{4.3}$$

where i increases in the radial and j increases in the azimuthal direction. Thus, for M_ϕ at the open circle points and for M_ρ at the triangle points, the metrics are simply the distances between points in the physical plane. When these metrics are needed at other points, simple averages are used. Thus at open circle points

$$M_\rho = \tfrac{1}{4}[M_\rho + M_\rho(j+1) + M_\rho(i-1) + M_\rho(i-1, j+1)]. \tag{4.4}$$

These definitions of the coordinates and metrics affect the definition of the finite-difference kinetic energy, but do not affect conservation of energy.

It is natural to form a finite-difference equation for Eq. (4.1) at the open circle points and one for Eq. (4.2) at the triangle points. Using simple centered differences and simple arithmetic averaging where required yields

$$\begin{aligned} &\frac{\partial}{\partial t}\left[\frac{-M_\rho}{HM_\phi}(\psi - \psi_{j-1})\right] - \frac{(1-\gamma)}{8}(P + P_{j-1})(\psi_{i+1} + \psi_{i+1,j-1} - \psi_{i-1} - \psi_{i-1,j-1}) \\ &\quad + \frac{\gamma}{8}(\psi + \psi_{j-1})(P_{i+1} + P_{i+1,j-1} - P_{i-1} - P_{i-1,j-1}) = \hat{\eta} - \hat{\eta}_{i+1}, \end{aligned} \tag{4.5}$$

$$\begin{aligned} &\frac{\partial}{\partial t}\left[\frac{M_\phi}{HM_\rho}(\psi - \psi_{i-1})\right] - \frac{(1-\gamma)}{8}(P + P_{i-1})(\psi_{j+1} + \psi_{i-1,j+1} - \psi_{j-1} - \psi_{i-1,j-1}) \\ &\quad + \frac{\gamma}{8}(\psi + \psi_{i-1})(P_{j+1} + P_{i-1,j+1} - P_{j-1} - P_{i-1,j-1}) = \hat{\eta} - \hat{\eta}_{j+1}. \end{aligned} \tag{4.6}$$

If one multiplies (4.5) by $\psi_{j-1} - \psi$ and (4.6) by $\psi - \psi_{i-1}$ and adds the two, one obtains the energy equation

$$\begin{aligned} &\frac{\partial}{\partial t}\left[\frac{M_\phi}{2M_\rho H}(\psi - \psi_{i-1})^2 + \frac{M_\rho}{2M_\phi H}(\psi - \psi_{j-1})^2\right] \\ &\quad = \frac{(1-\gamma)}{8}[(P + P_{j-1})(\psi_{i+1} + \psi_{i+1,j-1} - \psi_{i-1} - \psi_{i-1,j-1}) \end{aligned}$$

$$(\psi_{j-1}-\psi)+(P+P_{i-1})(\psi_{j+1}+\psi_{i-1,j+1}-\psi_{j-1}-\psi_{i-1,j-1})(\psi-\psi_{i-1})]$$

$$-\frac{\gamma}{8}[(\psi+\psi_{j-1})(P_{i+1}+P_{i+1,j-1}-P_{i-1}-P_{i-1,j-1})(\psi_{j-1}-\psi)$$

$$+(\psi+\psi_{i-1})(P_{j+1}+P_{i-1j+1}-P_{j-1}-P_{i-1,j-1})(\psi-\psi_{i-1})]$$

$$+(\hat{\eta}_{i+1}-\hat{\eta})(\psi-\psi_{i-1})-(\hat{\eta}_{i+1}-\hat{\eta})(\psi-\psi_{i-1}). \tag{4.7}$$

this equation vanish when summed over the basin as long as the stream function on the boundary is zero and an equation for the central stream function equation is obtained by summing Eq. (4.2) around the center. As in the continuous case, the normal mode solutions can be represented as $\psi(i,j,t)=\mathrm{Re}[\hat{\psi}(i,j)e^{i\sigma t}]$, where $\hat{\psi}$ is complex. This spatial discretization yields a tractable eigenvalue problem, there is thus no need to discretize the time derivative. The fact that energy is conserved ensures that σ is real.

In the next section, we will test these methods against exact solutions for closed basins, but first, it is useful to study their accuracy for the classical case of pure Rossby waves for a constant depth infinite plane. This eliminates the effect of the curvilinear coordinates and simplifies the Jacobian term. The vorticity equation is

$$\frac{\partial}{\partial t}\left(\frac{\partial^2\psi}{\partial x^2}+\frac{\partial^2\psi}{\partial y^2}\right)=-\beta\frac{\partial\psi}{\partial x}, \tag{4.8}$$

where $\beta=\partial f/\partial y$ is a constant.

Plane wave solutions of the form

$$\psi=e^{i(\kappa x+\lambda y+\sigma t)} \tag{4.9}$$

obey the dispersion relation

$$\sigma=\frac{-\beta\kappa}{\kappa^2+\lambda^2}. \tag{4.10}$$

With a uniform grid ($x=i\Delta x$, $y=j\Delta x$), the finite-difference equation is

$$\frac{\partial}{\partial t}(\psi_{i+1}+\psi_{i-1}+\psi_{j+1}+\psi_{j-1}-4\psi)$$

$$=-\frac{\beta\Delta x}{2}\left[\gamma(\psi_{i+1}-\psi_{i-1})+\frac{(1-\gamma)}{2}(\psi_{i+1,j+1}+\psi_{i+1,j-1}-\psi_{i-1,j+1}-\psi_{i-1,j-1})\right]. \tag{4.11}$$

The finite difference dispersion relation is

$$\sigma=\frac{-\beta(\sin\kappa\Delta x)/\Delta x)[\gamma+(1-\gamma)\cos\lambda\Delta x]}{[(2\cos\kappa\Delta x+2\cos\lambda\Delta x-4)/\Delta x^2]}. \tag{4.12}$$

The ratio of this frequency to the exact frequency is

$$S = \frac{(\sin \kappa\Delta x/\kappa\Delta x)[\gamma + (1-\gamma)\cos \lambda\Delta x]}{[(2\cos \kappa\Delta x + 2\cos \lambda\Delta x - 4)/(\kappa^2 + \lambda^2)\Delta x^2]}. \tag{4.13}$$

The numerator in this expression is the relative error in evaluating the Jacobian term; the denominator is the error in the Laplacian. The Laplacian is underestimated for all values of the wave numbers, κ and λ. Thus, to keep the ratio close to unity, one should choose a value of γ so that the Jacobian is underestimated by a similar factor. This, of course, cannot be done in general—for short x-wavelengths the ratio will be small no matter what the y-wavelength or choice of γ is. In fact, for an x-wavelength of $2\Delta x$ the ratio is zero.

Three values of γ are of particular interest because they correspond to three of Arakawa's Jacobians.

$$\gamma = 1 : J_4,$$
$$\gamma = 0 : J_3,$$
$$\gamma = 2/3 : J_7.$$

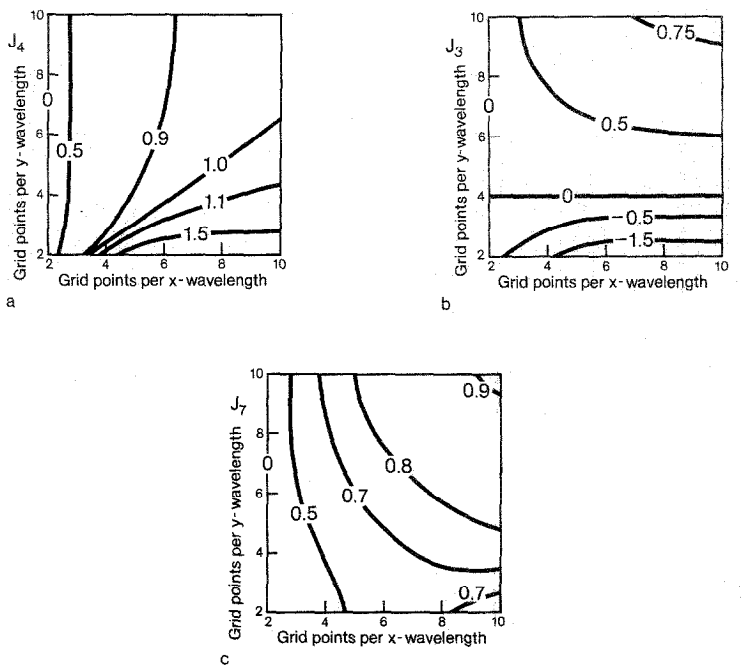

FIG. 2. S, ratio of finite difference frequency to the exact one for three forms of the Jacobian term. (a) $\gamma = 1$, (b) $\gamma = 0$, (c) $\gamma = 2/3$.

The numbering is from Arakawa [11]. J_4 is the simplest centered difference scheme. J_3 is the smplest form that can be derived from the original equations (2.1) and (2.2). J_7 is the form Arakawa recommends because it conserves not only kinetic energy and vorticity, as the others do, but also squared vorticity.

In Figs. 2a, b, and c we have plotted S, the ratio of the finite-difference frequency to the exact one versus the number of grid points per x-wavelength and the number of grid points per y-wavelength. The simplest scheme, J_4, is generally accurate except that the frequency is underestimated for short x-wavelengths and is overestimated for short y-wavelengths. J_3 is very inaccurate—the frequency is exactly zero for a y-wavelength of $4\Delta x$ and is negative for shorter waves. Arakawa's favorite scheme, J_7, underestimates the frequency for all wavelengths, but it is more consistent in that the error does not vary as much with wavelength as for the other two.

We found these conclusions to be true for the more complicated cases of the next section. The eigenfunctions were nearly the same no matter which scheme we used, and the frequencies were consistent with the results for pure Rossby waves. We chose to use J_4 because it is slightly more accurate for the large-scale modes.

5. Circular and Elliptic Tests

The infinite ocean beta-plane solutions of the previous section test the accuracy of the frequencies but not of the spatial structure of the modes or of the effects of the conformal mapping. The best test of the method requires a closed basin and thus a non-Cartesian coordinate system. Fortunately there are several exact solutions known.

The simplest case for which all the rotational modes are known is a circular basin with a uniform Coriolis parameter and a parabolic depth law. Since all the depth contours are concentric circles, the problem is separable in the azimuthal coordinate; the modes can be classified by the number of nodal diameters, m, and by the number of nodal circles, n. The nodal diameters and circles are curves other than the boundary for which the stream function is zero for a given time. Since the depth decreases monotonically from a maximum in the center to zero at the shore, all the modes propagate counterclockwise around the basin, the nodal circles remaining fixed and the nodal diameters rotating at a uniform rate. The frequency law [12, Sect. 212] is

$$\frac{f}{\sigma} = \frac{2(n+2)(m+n+1)}{m} - 1. \tag{5.1}$$

This number can be interpreted as the period expressed in units of the inertial period, $2\pi/f$. The shortest period, in the limit of large m, is three inertial periods. The period of the simplest mode, with one nodal diameter and no nodal circles, is seven inertial periods.

We computed these modes using 16 grid points in the longshore coordinate and 10 in the offshore coordinate. Equation (2.10) was discretized in ρ and ϕ using the finite

TABLE II

Computed and Theoretical Periods of Rotational Modes in a Circular Paraboloid. Theoretical Periods Are in Parentheses

	Nodal circles n				
Nodal diameters m	0	1	2	3	4
1	7.2 (7.0)	17.2 (17.0)	30.1 (31.0)	46.5 (49.0)	67.9 (71.0)
2	5.5 (5.0)	11.7 (11.0)	19.2 (19.0)	28.5 (29.0)	39.8 (41.0)
3	5.3 (4.33)	10.6 (9.0)	17.2 (15.0)	25.5 (22.3)	35.0 (31.0)
4	5.7 (4.0)	11.1 (8.0)	17.7 (13.0)	26.3 (19.0)	36.5 (26.0)
5	7.0 (3.8)	13.1 (7.4)	20.8 (11.8)	30.7 (17.0)	42.4 (23.0)

difference scheme discussed in the previous section with $\gamma = 1$. As in Section 4, there is no need to discretize the time derivative. The resulting numerical eigenvalue problem was solved by the technique of Moler and Stewart [16]. The computed and theoretical periods are presented in Table II for 25 of the simplest modes. As could be expected, the method is most accurate for the modes of large spatial scale. For the more complex modes, the method generally overestimates the period; this is consistent with the results of the infinite beta-plane of Section 4.

Another case for which all the normal modes are known is that of a circular basin of constant depth with a linear variation of the Coriolis parameter. Equation (4.8) written in polar coordinates is

$$\frac{1}{R\beta}\frac{\partial}{\partial t}\left[\frac{1}{r}\frac{\partial}{\partial r}r\frac{\partial\psi}{\partial r}+\frac{1}{r^2}\frac{\partial^2\psi}{\partial\theta^2}\right]+\cos\theta\frac{\partial\psi}{\partial r}-\frac{\sin\theta}{r}\frac{\partial\psi}{\partial\theta}=0. \tag{5.2}$$

The solutions of this equation that satisfy the boundary condition $\psi = 0$ on $r = 1$ are

$$\psi=\left\{\begin{matrix}\sin m\theta\\ \text{or}\\ \cos m\theta\end{matrix}\right\}J_m(Kr)e^{i(Kr\cos\theta+\sigma t)}, \tag{5.3}$$

where J_m is the Bessel function of the first kind and $K(m, n)$ is the inverse of its nth zero. The period of oscillation is

$$T(m,n)=\frac{2\pi}{\sigma}=\frac{4\pi K(m,n)}{R\beta}. \tag{5.4}$$

For this solution, the allowable range of m is 0 to ∞ and the range of n is 1 to ∞. For $m = 0$, there is only one solution for each value of n since sine $0 = 0$, but for $m > 0$ there are two solutions for each value of n. As in the case of the circular paraboloid, each mode has m nodal diameters. Unlike the paraboloid, the diameters are fixed in time. Each mode also has $n - 1$ nodal circles; thus the circular ocean is divided into $n \cdot (m + 1)$ independent sectors bounded by zero stream functions contours. Inside each of these sectors, the exponential function of Eq. (5.3) gives a westward phase propagation.

Because the finite-difference equations for the circular paraboloid are separable into products of azimuthal and radial functions, the solutions could be easily identified. This is not true for the circular beta-plane. As a consequence, we could classify only about six of the modes of largest space scale. The fundamental mode

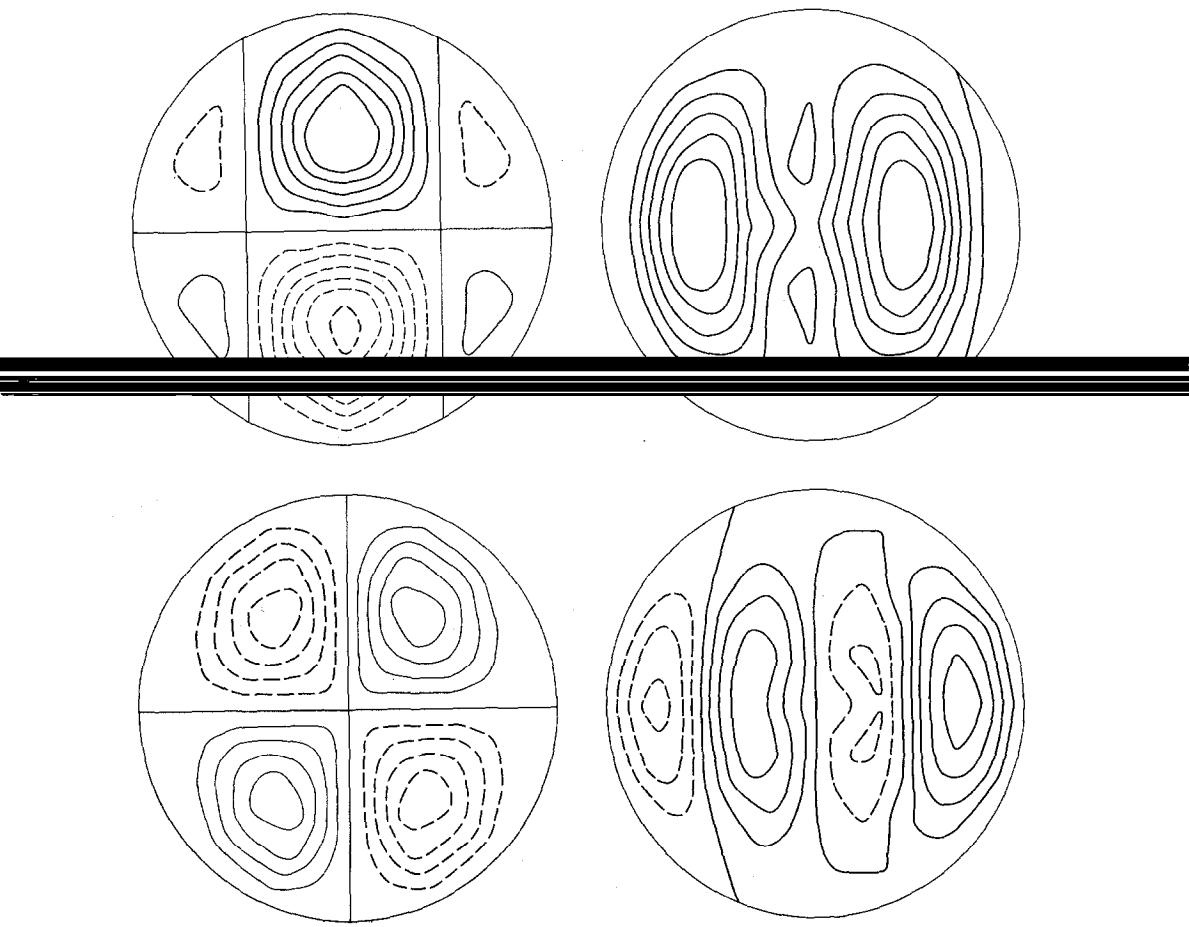

FIG. 3. Stream functions for rotational modes of the cricular beta-plane for $m = 1$, $n = 1$. Left—cosine mode. Right—sine mode. The top pattern is for one quarter period after the bottom pattern.

($m = 0$, $n = 1$) as given by Beardsley [9] has a computed period (in units of $1/R\beta$) of 31.7 compared to the theoretical value of 30.2. Figure 3 illustrates the pair corresponding to ($m = 1$, $n = 1$). The theoretical period is 48.2; the calculated periods are 52.6 for the cosine mode and 52.0 for the sine mode.

We turn our attention now to a more difficult problem—the calculation of the rotational modes of an elliptical paraboloid. This is the first problem in which we actually test the use of general orthogonal coordinates. There are two stages to the construction—the map onto the unit circle discussed in Section 3 and the choice of a suitable stretched version of the conformal coordinates. We make this choice purely on aesthetic grounds; the prettiest maps are usually the smoothest and thus probably minimize truncation error. The map for the 2×1 ellipse is given in Fig. 4.

Only a few of the rotational modes of an elliptic paraboloid are known, having been discovered by Ball [13]. The two simplest modes have periods of

$$\frac{f}{\sigma} = \sqrt{\frac{49 - 9p^2}{1 - p^2}}$$

and

$$\sqrt{\frac{25 - 10p^2}{1 - p^2}}, \tag{5.5}$$

where $p = (\varepsilon^2 - 1)/(\varepsilon^2 + 1)$ and ε is the ratio of the major axis to the minor axis. These two reduce to the two circular paraboloid modes with no nodal circles and one

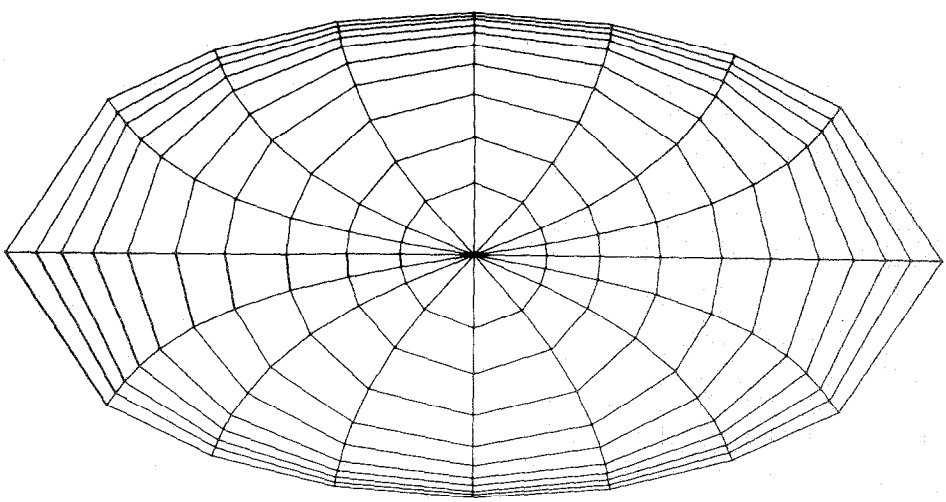

FIG. 4. Numerical grid for 2×1 ellipse generated by conformal mapping procedure.

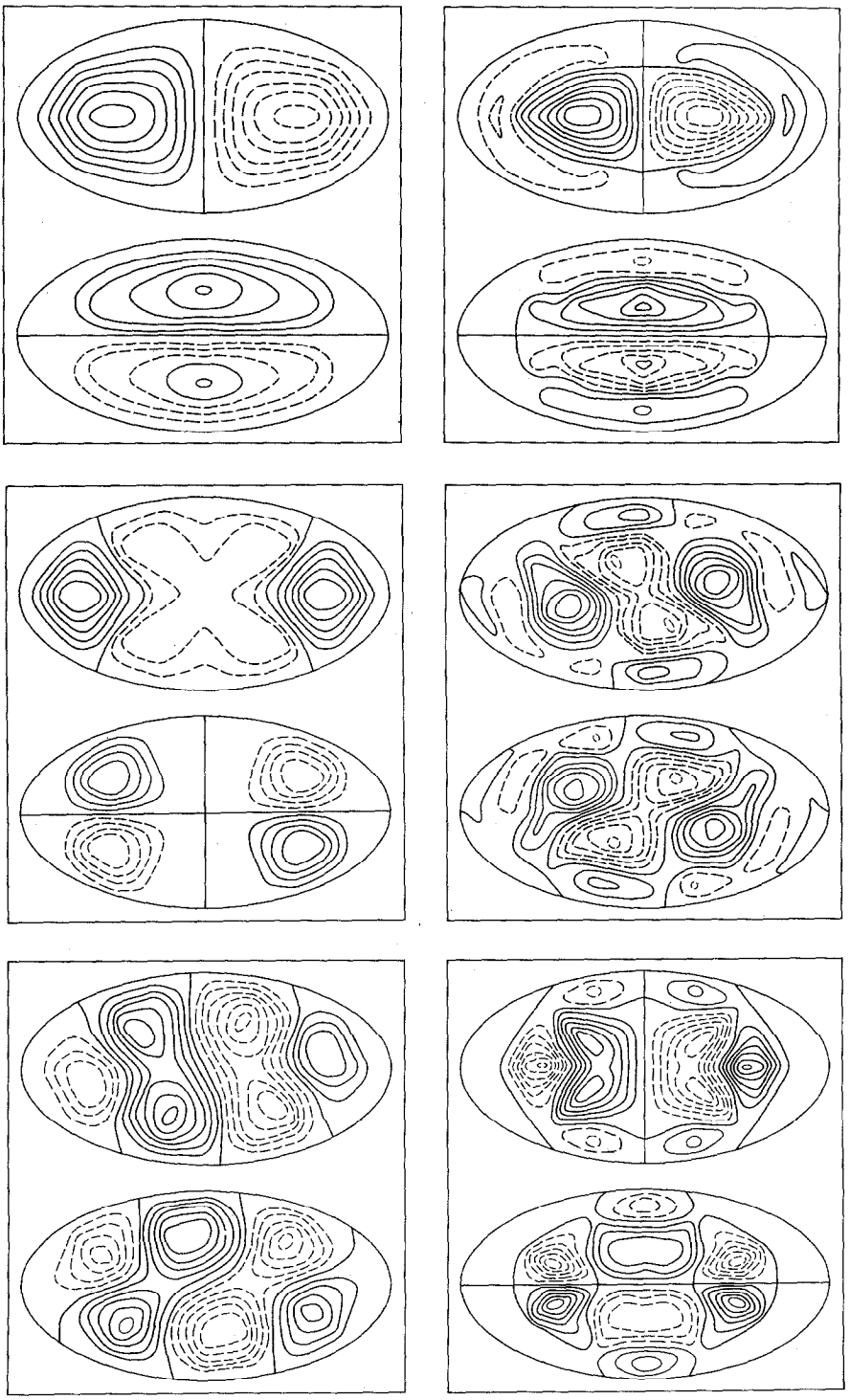

FIG. 5. Stream functions for the rotational modes of the elliptic paraboloid. In each box the top pattern is for one-quarter period after the bottom pattern. The periods are given in Table III.

TABLE III

Computed and Some Theoretical Periods of Rotational Modes in a 2×1 Elliptic Paraboloid. Theoretical Periods are in Parentheses

	Radial structure n	
Azimuthal structure m	0	1
1	8.42 (8.46)	21.8 (20.9)
2	6.33 (5.78)	14.7
3	5.65 (4.85)	14.2

and two nodal diameters, respectively. For an ellipse twice as long as it is wide ($\varepsilon = 2$), these periods are 8.46 and 5.78 compared to 7.0 and 5.0 for the circle.

Ball also gives an equation that can be used to calculate two more modes

$$\mu^4[(221 - 45p^2)^2 - 104^2p^2] - 2\mu^2(1 - p^2)(1385 - 153p^2) + 9(1 - p^2)^2 = 0, \quad (5.6)$$

where $\mu = \sigma/f$. For the circle, these have periods of 17 and 4.33 inertial periods. For the 2×1 ellipse, the periods are 20.9 and 4.85. One can see from Table II that the longer period mode should have one nodal circle and one nodal diameter and the short period mode should have no nodal circles and three nodal diameters.

From the structures of the first two modes given in Figs. 1 and 2 of Ball's paper and the structures in the last two modes in a circular basin, we have identified all four of these modes in our calculations. We have also been able to identify two more calculated modes that seem to have the correct structures and periods to complete the 2×3 matrix of modes given in Fig. 5. These six modes correspond to the upper left-hand corner of Table II, with "radial" structure increasing to the right and "azimuthal" structure increasing downwards. The calculated periods, with Ball's theoretical periods in parentheses, are given in Table III. Note that the error is comparable to that of the circular paraboloid and that for all the modes the periods are larger for the ellipse than for the circle.

6. Conclusions

The method for calculating rotational modes presented in this paper has produced good results for several analytical basins. The effect of truncation errors on computed frequencies is small for modes with large spatial scales, but increases rapidly with

more complicated structures. Rotational mode periods in the circular and elliptical paraboloids tend to decrease with increasing azimuthal structure and increase with increasing radial structure. Computed frequencies deviate from this pattern as spatial structure becomes more complicated.

We developed the numerical method with the goal of computing rotational modes in the Great Lakes. The method is general enough to apply to arbitrary topography, but it is seen that especially elongated basins are not amenable to this treatment as truncation errors become significant both in the conformal mapping procedure and in the eigenvalue problem. For elongated lakes or complex basin shapes, coordinates generated in this manner would correspond to a very uneven distribution of grid points in the physical plane and it might be better to use the finite element method of Platzman [14] or the triangular finite difference mesh of Thacker [17].

At present, the most promising set of observations that might be used to verify techniques for computing rotational modes are those of Saylor *et al.* [15] for Lake Michigan. Unfortunately, Lake Michigan is long and has a complex topography with two major basins. Perhaps a basin with a simpler topography like Lake Kinneret or the Black Sea, will be a better proving ground for the calculation and observation of rotational modes.

REFERENCES

1. D. J. SCHWAB, *Mon. Weather Rev.* **106** (1978), 1476.
2. D. J. SCHWAB, *in* "Symposium on Long Waves in the Ocean, Manuscript Report Series No. 53," p. 140, Marine Sciences Directorate, Department of Fisheries and the Environment, Ottawa, 1979.
3. G. W. PLATZMAN, *J. Phys. Oceanogr.* **2** (1972), 117.
4. D. B. RAO AND D. J. SCHWAB, *Philos. Trans. R. Soc. London Ser. A* **281** (1976), 63.
5. J. R. BENNETT, *J. Phys. Oceanogr.* **8** (1978), 1095.
6. L. H. SWINFORD, *in* "Construction and Applications of Conformal Maps" (E. F. Beckenbach, Ed.), Nat. Bur. Standards Appl. Math. Series No. 18 (NTIS), 1952.
7. Z. NEHARI, "Conformal Mapping," McGraw–Hill, New York, 1952.
8. M. ABRAMOWITZ AND I. A. STEGUN, "Handbook of Mathematical Functions," U.S. Govt. Printing Office, Washington, D.C., 1964.
9. R. C. BEARDSLEY, *J. Comput. Phys.* **7** (1971), 273.
10. A. ARAKAWA, *J. Comput. Phys.* **1** (1966), 119.
11. A. ARAKAWA, *in* "Numerical Solutions of Field Problems in Continuum Physics," Durham, N. C. (G. Birkhoff and S. Varga, Eds.), p. 24, Amer. Math. Soc., Providence, R.I., 1970.
12. H. LAMB, "Hydrodynamics," 6th ed., Cambridge Univ. Press, Cambridge, 1932.
13. F. K. BALL, *J. Fluid Mech.* **23** (1965), 545.
14. G. W. PLATZMAN, *J. Phys. Oceanogr.* **8** (1978), 323.
15. J. H. SAYLOR, J. C. K. HUANG, AND R. O. REID, *J. Phys. Oceanogr.* **10** (1980), 1814.
16. C. B. MOLER AND G. W. STEWART, *SIAM J. Numer. Anal.* **10** (1973), 241.
17. W. C. THACKER, *J. Phys. Oceanogr.* **8** (1978), 680.